Heliyon 11 (2025) e42502

Contents lists available at ScienceDirect

Heliyon

journal homepage: www.cell.com/heliyon

Research article

Optimizing the design of a pediatric blood pump through orthogonal experimentation

Kaiyun Gu [a,b,*], Kaiyue Yang [b,**], Changlong Zhao [b], Qiang Shu [a], Ru Lin [a,***]

[a] Department of Cardiac Surgery, Children's Hospital, Zhejiang University School of Medicine, National Clinical Research Center for Child Health, Hangzhou, China
[b] Department of Innovation Center for Child Health, Binjiang Institute of Zhejiang University, Hangzhou, China

ARTICLE INFO

Keywords:
Pediatric heart failure
Axial blood pump
Hemodynamics
Orthogonal experiment
Blade parameters

ABSTRACT

Background: Pediatric heart failure patients weighing less than 30 kg are prioritized for small axial flow blood pumps due to their smaller body size. This study aims to optimize the blade design of pediatric axial flow blood pumps by conducting orthogonal experiments on blade parameters and integrating hydraulic experiments with hemodynamic numerical simulations, so as to improve the hydraulic performance of pediatric blood pumps while reducing blood damage.

Methods: This study employs a combination of computational fluid dynamics (CFD) and orthogonal experimentation to optimize six key parameters of the impeller blade. The optimal blade parameter model is determined through range analysis. The hydraulic performance of the optimized model is evaluated via in vitro experiments, which provide pressure and flow data. Additionally, hemodynamic performance is assessed using CFD, with key evaluation indices including flow field characteristics, pressure distribution, and shear stress distribution within the axial flow pump.

Results: From an orthogonal experiment, six blade parameters were found to influence blood pump pressure head: the distance between the starting surface of the blade and the hub (W), blade height (h), blade length (L), blade wrapping angle (α), blade outlet angle (β), and blade inlet angle (γ). The approximately linear pressure-flow curve of the optimized axial blood pump meets design requirements at a pump speed of 10000 rpm, achieving a pressure head of 50.8 mmHg and a flow rate of 3L/min. Computational fluid dynamics analysis reveals a smooth flow field with a low maximum reflux rate of 0.16 % in sections I, II, and III. Pressure is evenly distributed, with a maximum of approximately 10^4Pa in the inner wall of the impeller area, working face of the impeller blade, and guide tail blade. There are no high shear stress areas, with shear stress below 200Pa accounting for approximately 95.08 % and areas exceeding 300Pa accounting for roughly 1.56 %.

Conclusions: This study investigates the correlation between blade parameters and hydraulic performance in axial flow pumps used for blood pumping. The results of both flow field analysis and experimental studies, conducted using orthogonal experiments, demonstrate that the optimized blood pump exhibits enhanced performance in reducing both reflux rate and shear stress.

* Corresponding author. Department of Cardiac Surgery, Children's Hospital, Zhejiang University School of Medicine, National Clinical Research Center for Child Health, Hangzhou, China.
** Corresponding author.
*** Corresponding author.
E-mail addresses: gukaiyun@zju.edu.cn (K. Gu), yangky7@163.com (K. Yang), linru.008@163.com (R. Lin).

https://doi.org/10.1016/j.heliyon.2025.e42502
Received 4 May 2023; Received in revised form 27 November 2024; Accepted 5 February 2025
Available online 6 February 2025

These findings provide valuable insights for the design optimization of pediatric ventricular assist devices.

1. Introduction

Heart failure (HF) is a complex clinical syndrome associated with abnormalities in cardiac structure or function [1,2]. The main causes of HF in children are congenital malformations and cardiomyopathy, as reported by the World Health Organization in 2009. In the US, 11,000–14,000 children are hospitalized annually due to HF, with a mortality rate of 7 % [3]. The incidence of HF in children is 0.87/100,000 in the United Kingdom and Ireland [4] and 7.4/100,000 in Taiwan [5]. Unfortunately, one third of children with HF die or require transplantation within one year of diagnosis.

Pediatric use of ventricular assist devices (VADs) as a bridge to transplantation (BTT) is increasing [6]. The Pediatric Heart Transplant Study reported that VAD support resulted in 17 % mortality and 76 % transplantation [7]. Positive outcomes, including survival on the device, bridge to transplantation, and recovery, were observed in 82 % of pediatric patients at 6 months [8,9]. Currently, one-third of pediatric heart transplantations involve VAD support, which has garnered significant attention. The Berlin Heart EXCOR pediatric VAD is approved by the Food and Drug Administration for BTT in children. Kaplan-Meier post-transplantation survival did not differ between EXCOR cohort and without pretransplant mechanical circulatory support cohort [10]. The Infant Jarvik 2015 device may be considered a suitable option for implantation in patients weighing less than 8 kg, owing to its inherent stability and ability to sustain optimal patient hemodynamics [11] and has been shown to be effective in inducing recovery in those with dilated cardiomyopathy [12].

Advancements in technology have improved the performance of VADs, leading to increased focus on the computational fluid dynamics (CFD) analysis in related research. For instance, Li et al. used computational fluid dynamics to investigate the impact of blade number, angle, and thickness on the pressure head, hemolysis, and platelet activation of a centrifugal blood pump [13]. Wiegmann et al. systematically varied the design parameters of a centrifugal blood pump and analyzed the effects of these changes on flow field and hydraulic performance using CFD [14]. Similarly, Tompkins et al. optimized the fluid structure and analyzed the hydraulic performance of a magnetic levitation rotary blood pump designed for pediatrics using CFD [15]. Bozi et al. employed CFD to study the blood compatibility of axial flow pumps with two impeller designs, analyzing pressure and velocity vector distribution in the axial flow pump and predicting platelet activation caused by abnormal shear stress history [16]. Thamsen et al. combined CFD with particle image velocimetry to study the flow field of HeartMate3 [17], while Chang et al. employed CFD to study the mechanical and hemolytic properties of four different commercial axial flow pumps [18]. Antaki et al. used reduced-order formulas to allow rapid optimization of key design parameters; then rigorous CFD and FEA simulations were carried out to develop children's blood pumps [19]. Kannojiya et al. used computational fluid dynamics software to conduct a three-dimensional study of an impeller with three curved and helical blades within a certain range of rotational speed and flow rate [20]. They found that the helical blades avoided mixing of different blood flows, thereby reducing eddy current losses. Ghadimi et al. combined metamodel assisted genetic algorithm with CFD to optimize the impeller and volute geometries of a typical centrifugal blood pump [21]. The above studies have explored the performance and optimization methods of VADs. This study adopts a new design optimization method for pediatric blood pump.

For the design of blood pumps, the structural parameters of the impeller are crucial to the performance of the blood pump [12,22,23]. Designers need to obtain the best combination of blade parameters through numerical calculations and experiments. However, during the impeller optimization process, it is a huge workload to study the influence of specific parameters on the performance of the blood pump by changing one parameter of the blade at a time. As a multi-factor and multi-objective optimization design method, orthogonal experiment method is applied to the optimization design of pumps, which effectively solves the problem of long model test period [24–26]. Chen designed an orthogonal experiment for the hydraulic levitation structure of the blood pump to study the effects of groove width ratio, groove depth, gap and other parameters on the blood compatibility of the blood pump [27]; Huo optimized different blade parameters of the magnetic levitation centrifugal pump through orthogonal experimental methods, which greatly reduced the turbulence intensity of the blood pump and significantly improved the hydraulic and hemolytic performance of the blood pump [28]. Based on the single-factor experimental results, Feng selected three structural parameters and used the orthogonal experimental method to conduct simulation calculations on different parameter schemes in order to achieve the optimal design of the rolling blood pump structure [29]. However, due to the unique physiological characteristics of children, such as smaller heart and chest volumes and higher blood compatibility requirements compared with adults, the design of pediatric blood pumps is more challenging.

This study optimizes the ventricular assist device (VAD) for children under 30 kg using an axial flow structure. Six impeller blade parameters are optimized using CFD and orthogonal experiments. The resulting model is evaluated for hydraulic performance through in vitro experiments and hemodynamic performance using CFD to determine flow field, pressure distribution, and shear stress distribution.

2. Materials and method

2.1. Baseline blood pump design

The baseline blood pump is designed for children under 30 kg, limiting its overall size. Combined with the advice of clinicians, 3L/

min and 40 mmHg is selected as the design work point of the blood pump. The outer diameter of the baseline pump is 12.1 mm and the length is 40 mm. Fig. 1A is a schematic diagram of the overall dimensions of the blood pump. Fig. 1B shows the schematic diagram of the pump impeller and key blade parameters, including an outer diameter of 11 mm, length of 24 mm, and three blades designed using streamline methods. To enhance the blood pump's performance, it's essential to optimize the impeller design, the core component.

2.2. Mesh details and sensitivity analysis

The calculation model consists of three sections with two static and dynamic interfaces each: the static guide head, guide tail area, and rotating impeller area. We used an unstructured grid with a boundary layer at the fluid-solid interface and higher grid density near the blade to obtain accurate local velocity gradients. After performing a grid independence analysis (Table 1), we selected a grid setting of 10 million to balance computational accuracy and resources (Fig. 2).

2.3. CFD analysis

The hydraulic and hemolytic performance of all blood pump models was evaluated using CFD simulations. The CFD simulations were conducted with the commercial software Ansys Fluent, solving the incompressible Navier-Stokes equations (1) and (2) using the SIMPLE method.

The N-S equation is as follows:

$$\nabla u = 0 \tag{1}$$

$$\rho\left(\frac{\delta u}{\delta t}\right) + \rho u \bullet \nabla u = \nabla\left[-pI + \mu\left(\nabla u + (\nabla u)^{T}\right)\right] + F \tag{2}$$

Where the blood velocity (u), pressure (p), dynamic viscosity (μ), blood density (ρ), and volume force field (F) play crucial roles in understanding the mechanics of blood flow.

In this study, the SST k-ω turbulence model was employed to deal with y^{+} may exceed 1 at some locations, and the turbulence and momentum were solved using the second-order upwind method to ensure high accuracy in the calculations. The transport equations (3) and (4) expressions of the SST k-ω model are presented below.

$$\frac{\partial k}{\partial t} + u_j\frac{\partial k}{\partial x_j} = \frac{\partial}{\partial x_j}\left[\left(\nu + \frac{\nu_t}{\sigma_{k_3}}\right)\frac{\partial k}{\partial x_j}\right] + G_k - \beta' k\omega \tag{3}$$

$$\frac{\partial \omega}{\partial t} + u_j\frac{\partial \omega}{\partial x_j} = \frac{\partial \omega}{\partial x_j}\left[\left(\nu + \frac{\nu_t}{\sigma_{\omega_3}}\right)\frac{\partial \omega}{\partial x_j}\right] + \alpha_3\frac{\omega}{k}G_k - \beta_3\omega^2 + 2(1-F_1)\frac{1}{\sigma_{\omega_2}\omega}\frac{\partial k}{\partial x_j}\frac{\partial \omega}{\partial x_j} \tag{4}$$

Where the turbulent kinetic energy (k), time(t), Turbulent kinetic energy generated by laminar velocity gradient (G_k), Coefficient (α,β), specific dissipation rate (ω), weighting function (F_1)

The blood flow through the VAD is analyzed using a weighting function F_1. Blood is assumed to be an incompressible Non-

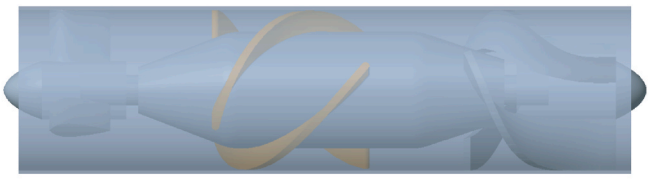

A

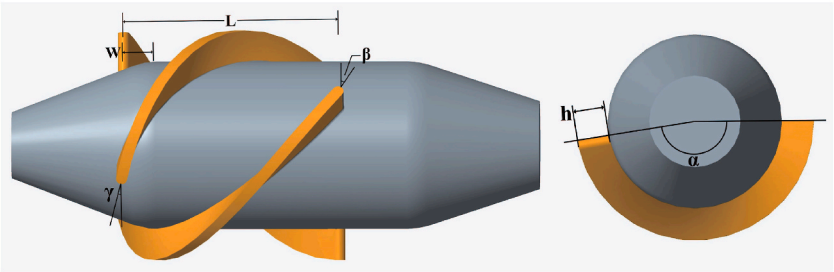

B

Fig. 1. (A) 3D model of the baseline blood pump; (B) Diagram of key parameters of the blood pump blades.

Table 1
Results of the grid-independence test.

Number of fluid grid($\times 10^6$)	Pressure Head (mmHg)	Relative error	Mean y^+ on impeller surface
6.02	44.1	–	1.5762
8.03	42.9	2.72 %	1.2909
10.01	40.2	2.70 %	0.9465
13.04	40.6	0.99 %	0.6213

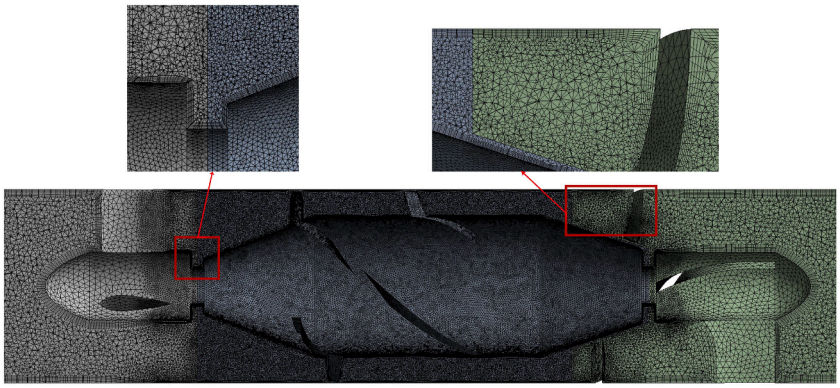

Fig. 2. Mesh grid division diagram of the blood pump fluid domain.

Newtonian fluid with a density of 1050 kg/m^3 and a dynamic viscosity of 0.0035 Pa s [30]. The momentum equation residual is used to determine convergence, with a tolerance of 10^{-4}. The inlet boundary condition is zero pressure, while the outlet boundary condition is a flow rate of 3 L/min (0.0525 kg/s), all the solid walls were assumed no-slip and adiabatic. To ensure fully developed flow, the inlet and outlet lengths are extended to 10 times the diameter. Rigid body rotation of the rotor blade is achieved using a rotating coordinate system.

2.4. Hemolysis predictions

Hemolysis, the rupture or destruction of red blood cells, is determined by the magnitude and duration of shear force exerted on them. The hemolysis index (HI) is used to quantify the degree of hemolysis. Taskin et al. developed a power law model based on numerous experiments to investigate the relationship between HI and shear force/time [31]. The model establishes an empirical formula (5) to describe this relationship.

$$\mathrm{HI} = C\tau^a t^b \tag{5}$$

The parameters obtained after fitting are as follows: $C = 1.21 \times 10^{-5}$,a = 2.004,b = 0.747.

This study uses a power law model and the Lagrange model established by Garon et al. to calculate hemolysis in blood pumps [32]. The hemolysis index is obtained by averaging 1200 streamlines. Equation (6) expresses the Lagrange model used to quantify hemolysis.

$$\mathrm{HI} = C\left(\sum_{inlet}^{outlet} \Delta t \tau^{a/b}\right)^b \tag{6}$$

The calculation equation (7) of the shear force τ is as follows:

$$\tau = \left[\frac{1}{6}\sum\left(\tau_{ii} - \tau_{jj}\right)^2 + \sum {\tau_{ij}}^2\right]^{1/2} \tag{7}$$

Arvand et al. and Ge et al. have shown that Reynolds stress, a statistical measure, is not directly related to the physical force on blood cells [33,34]. Therefore, the equation for calculating shear force only considers viscous shear force.

2.5. Orthogonal experimental design

In the design process of the pediatric blood pump, on the one hand, there are limitations in the external dimensions, and on the other hand, it needs to meet the performance requirements of the pump. Therefore, multi-objective and multi-parameter optimization design of the blood pump is required. The orthogonal experimental method is a powerful way to study multiple factors and levels [35]. When there are three or more factors involved in the experiment, and there may be interactions between factors, the workload of the

experiment will become very large, or even difficult to implement. In view of this problem, orthogonal experimental design is undoubtedly a better choice [36]. In this study, six factors were selected for pump blade design: blade inlet angle (γ), blade outlet angle (β), blade wrapping angle (α), blade length (L), blade height (h), and distance between blade starting surface and hub (W), each with five levels. Without orthogonal design, 15,625 combined experiments would be required for a comprehensive investigation. However, by employing orthogonal design principles, we created a factor-level table and designed 25 groups of orthogonal experimental combinations, as shown in Table 2. Orthogonal experiments can achieve results equivalent to a large number of comprehensive experiments with the minimum number of tests. Therefore, the application of orthogonal table design experiments is an efficient, fast and economical multi-factor experimental design method [37].

The orthogonal experimental method uses range analysis, also known as the R method. By calculating the R value, this approach assesses the efficacy and performance of a factor in achieving the optimal outcome. In range analysis, K-avg refers to the average value of experimental data at a certain level of a certain factor; the optimum level refers to the level number corresponding to the best K-avg value of a certain factor; R refers to the range value of the factor, that is, The maximum value of K-avg minus the minimum value of K-avg, the factor range value can compare the influence of each factor on the design goal. Ultimately, it facilitates the identification of the optimal combination of factors.

2.6. Hydraulic experiment

An experimental hydraulic performance test was conducted on the platform shown in Fig. 3 (A, B) to validate the accuracy of CFD simulation and determine the hydraulic performance of the blood pump. The test employed a blood viscosity of 3.5 mPa s at a simulated room temperature of 24 °C, consisting of a 2.3:1 mixture of 0.9 % sodium chloride solution and glycerol. An ultrasonic flow sensor (measurement accuracy is 0.5 %–1 %) was placed upstream of the blood pump inlet to measure the flow rate, while pressure sensors (measurement accuracy is 1 %) were installed at the inlet and outlet of the pump. A damping valve was located downstream of the pressure gauge at the outlet of the blood pump.

3. Results

Through 25 sets of CFD simulation results, we can obtain the blood pump pressure heads under different orthogonal experimental combinations, as shown in Table 2. It can be seen that the hydraulic performance of the pump is significantly affected by the combination of blade parameters at a constant speed of 12000 rpm and a flow rate of 3 L/min. Only six of these sets (test numbers 3, 10, 11, 14, 18, 22) satisfied the design requirement of 40 mmHg for pressure head. Range analysis of the results revealed the degree of influence of each blade parameter on the pump's hydraulic performance. Larger ranges indicate greater effects, while smaller ranges suggest lesser impacts. This analysis provided insight into the order of influence of blade parameters on pump head, serving as a reference for optimal blade design.

Table 3 ranks the blade parameters by their influence on pump head, from greatest to least: distance between blade starting surface and hub (W), blade height (h), blade length (L), blade wrapping angle (α), blade outlet angle (β), and blade inlet angle (γ). The greater

Table 2
Orthogonal experimental combination and result of pressure head.

Serial number	γ (°)	β (°)	α (°)	L (mm)	h (mm)	W (mm)	Pressure Head (mmHg)
1	10	10	130	6	1	−5	20
2	15	25	130	10	1.8	1	25
3	20	40	130	14	1.6	−3	45
4	25	55	130	8	1.4	3	10
5	30	70	130	12	1.2	−1	14
6	30	10	150	14	1.4	1	8
7	10	25	150	8	1.2	−3	29
8	15	40	150	12	1	3	−5
9	20	55	150	6	1.8	−1	24
10	25	70	150	10	1.6	−5	79
11	25	10	170	12	1.8	−3	58
12	30	25	170	6	1.6	3	6
13	10	40	170	10	1.4	−1	18
14	15	55	170	14	1.2	−5	51
15	20	70	170	8	1	1	−12
16	20	10	190	10	1.2	3	3
17	25	25	190	14	1	−1	8
18	30	40	190	8	1.8	−5	72
19	10	55	190	12	1.6	1	19
20	15	70	190	6	1.4	−3	7
21	15	10	210	8	1.6	−1	20
22	20	25	210	12	1.4	−5	53
23	25	40	210	6	1.2	1	−36
24	30	55	210	10	1	−3	9
25	10	70	210	14	1.8	3	16

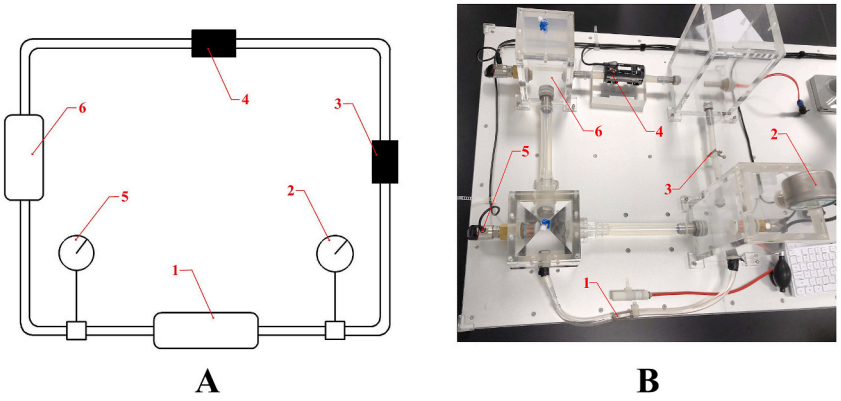

Fig. 3. Test loop. (1) Pump; (2) outlet pressure manometer; (3) Clamp; (4) Flowmeter; (5) inlet pressure manometer; (6) reservoir. (A) shows the schematic of the test loop; (B) shows the actual photo of the test loop.

the range value R of a factor, the greater the influence of the factor on the design objective.

Fig. 4(A–F) shows the impact of blade parameters on the pressure head of the blood pump. The pressure head initially decreases and then increases with increasing blade inlet angle γ, reaching a maximum at γ1. Similarly, the pressure head increases and then decreases with increasing blade outlet angle β, peaking at β3. The pressure head follows a similar trend with increasing blade wrap angle α, reaching a maximum at α2. Increasing blade length L initially increases the pressure head, but beyond L4, the pressure head decreases. The maximum pressure head is achieved at h5 when increasing blade height h. Finally, the pressure head decreases and then increases with increasing distance w between the blade starting surface and the hub, with the maximum pressure head occurring at W1.

The combination of blade parameters γ1β3α2L4h5W1 generally maximizes pump head (model A). However, the design of a blood pump must also consider requirements for hemodynamics and hemolysis.

Through three-dimensional modeling and CFD simulations of blade parameters (model A), we found that at a rotational speed of 12000 rpm and flow rate of 3 L/min (condition A1), the blood pump pressure head exceeded the design requirement of 40 mmHg, reaching 85 mmHg. However, high pump speeds can increase hemolysis. To reduce hemolysis, we propose reducing the speed for condition A1 in model A. After several CFD simulations, we determined that the optimal blade parameters are achieved at a speed of 10000 rpm and flow rate of 3 L/min (condition A2), producing a pressure head of 52 mmHg, meeting the design requirements.

We compared the calculation results of the conditions A1 and A2 of model A, the 6 serial numbers of models (numbered 3, 10, 11, 14, 18, and 22) that met the design requirements in 25 groups of orthogonal experiments, and the baseline pump under the design conditions (12000 rpm), as shown in Fig. 5.

Under the conditions of 12000 rpm and 3L/min, Model A achieved a pressure head of 85 mmHg, while the baseline pump achieved 40.3 mmHg, indicating that the optimal blade parameters from the orthogonal experiment significantly improved pump pressure head. Hemolysis values (HI) were calculated for each model, with Model 18 having the highest (23.63×10^{-4}) and the lowest observed in A2 (10,000 rpm and 3 L/min) at 11.65×10^{-4}, which was 48 % lower than the baseline pump hemolytic value.

Fig. 6 is impeller experimental model (A) and the experimental results and simulation results of the blood pump at different speeds (B). At flow conditions of 12000 rpm and 3 L/min, the pressure head was 83.9 mmHg, with a 1.3 % error relative to the CFD simulation results (85 mmHg). At flow conditions of 10000 rpm and 3 L/min, the pressure head was 50.8 mmHg, with a 3.5 % error relative to the CFD simulation (52 mmHg).

The error between the simulation results and the experimental results may come from many aspects, such as the grid, calculation model and boundary conditions in the process of simulation calculation, and may also come from the sensor accuracy, experimental data processing error and sensor accuracy in the process of experiment. Nonetheless, the errors between the experimental and CFD simulation results remained below 5 %, confirming the simulation model and grid settings' rationality.

Fig. 6A shows the actual picture of the impeller. Fig. 6B shows that the pressure head decreases with the increase of flow at constant flow and speed. The relationship between pressure head and flow rate remains approximately linear without distortion points throughout the entire operating range, indicating reliable pump performance. The pump achieves a maximum rotational speed of 12000 rpm, a flow rate of 6.8 L/min, and a pressure head of 105 mmHg, meeting clinical requirements for pediatric ventricular assistance.

Fig. 7 illustrates the flow distribution of model A at a speed of 10000 rpm and 3 L/min, mimicking blood flow through the pump. When blood flows through the blades, it generates a small backflow due to the impact, as seen in Fig. 7A and D. This reflux flow helps

Table 3
Range analysis results of orthogonal experiment.

Factor	γ	β	α	L	h	W
R	12.4	14.4	30.4	38.6	48.2	73.0
Optimum level	1	3	2	4	5	1

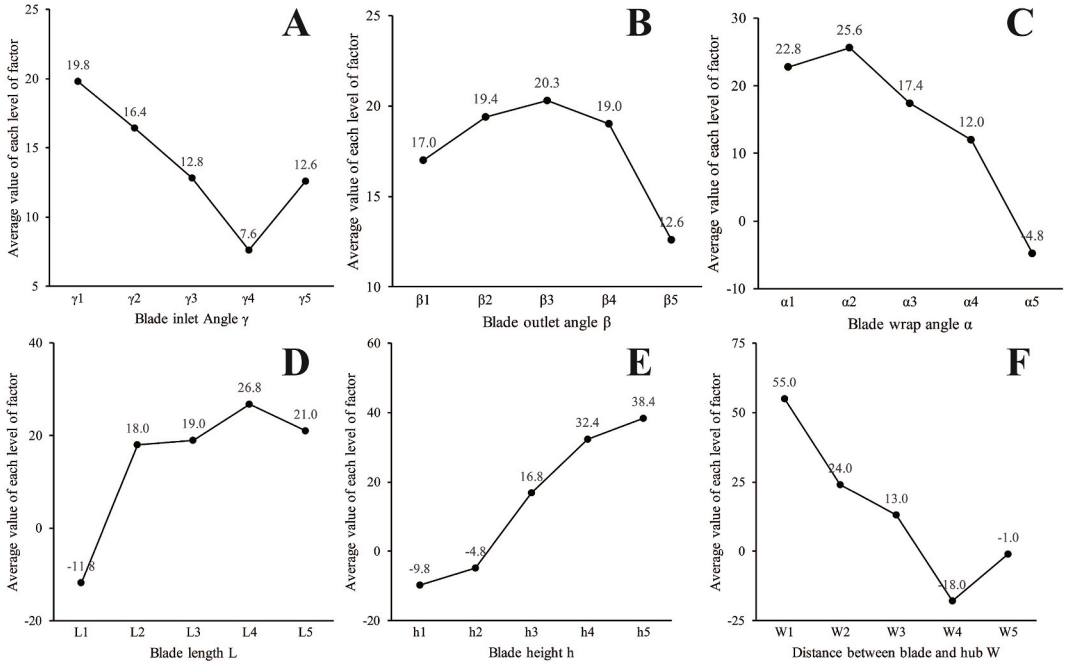

Fig. 4. The effect of impeller blade parameters on the blood pump's pressure head. (A) The effect of blade inlet angle γ on the pressure head; (B) The effect of blade outlet angle β on the pressure head; (C) The effect of blade wrap angle α on the pressure head; (D) The effect of blade length L on the pressure head; (E) The effect of blade height h on the pressure head; (F) The effect of distance between the blade starting surface and the hub W on the pressure head.

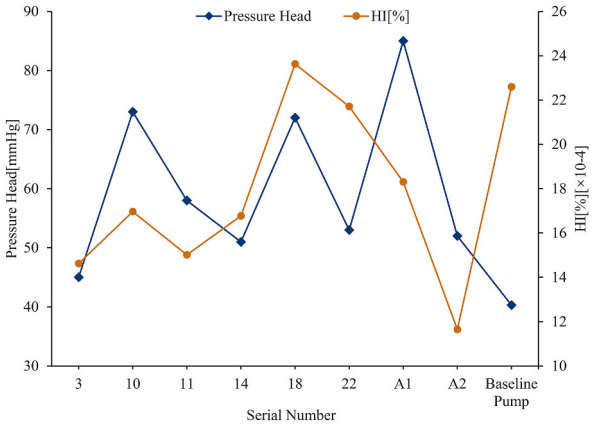

Fig. 5. Comparison of hydraulic performance and hemolytic performance.

clean the area near the guide head and prevent thrombosis. Likewise, when blood flows through the guide vane, it also returns due to impact, as shown in Fig. 7B and E.

To quantify blood backflow in a pump, we define the reflux coefficient R as the ratio of mass flow from the outlet to the inlet on a specific section to the total section mass flow. formula (8) for calculating R is as follows:

$$R = \frac{M_{out-in}}{M_{total}} \times 100[\%] \tag{8}$$

Where R is the reflux coefficient, M_{out-in} is the mass flow rate from the outlet to the inlet direction on the section, and M_{total} is the total mass flow rate on the section.

In this study, we evaluated blood flow backflow in the pump by analyzing three sections (I, II, and III) shown in Fig. 7C. Table 4 indicates that the maximum return flow rate on section II is 0.16 %, which is caused by blade impact during blood flow through the impeller. However, this small backflow does not affect the pump's performance.

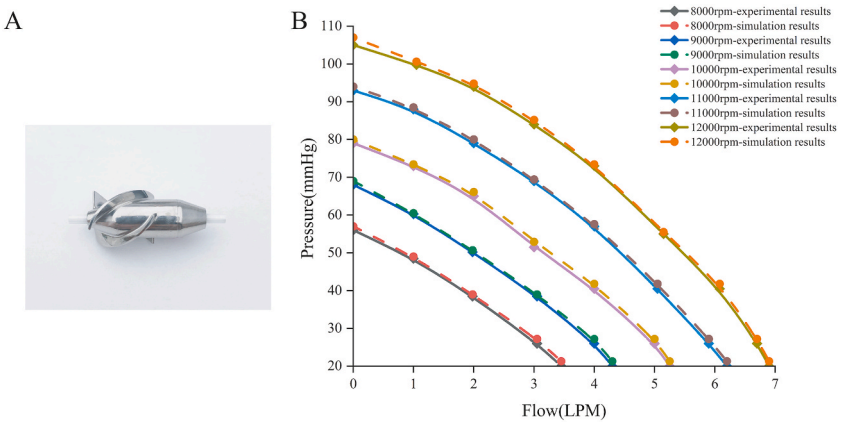

Fig. 6. (A) The actual picture of the impeller; (B) Performance curves of the blood pump from simulation and experiment.

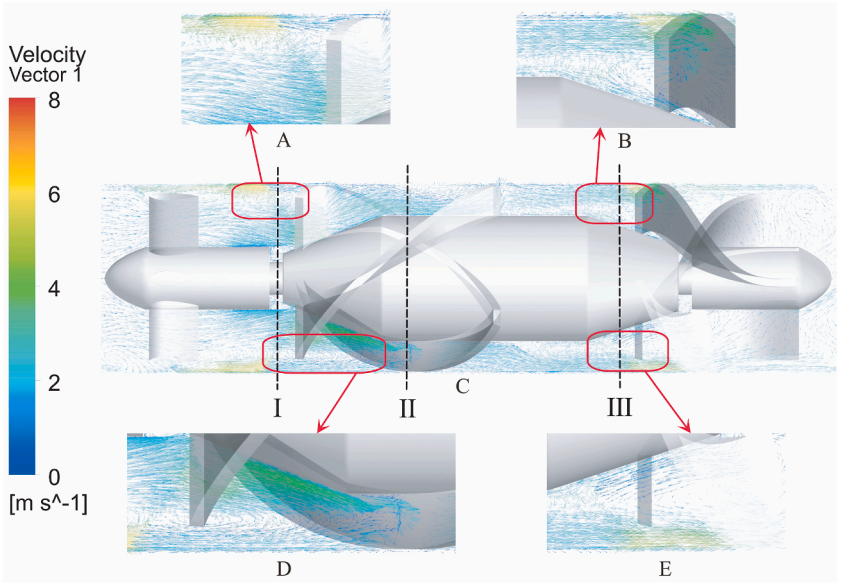

Fig. 7. (C) Flow field distribution of blood pump. (A, B, D, E) Detailed view of the flow field region in the blood pump.

Fig. 8 depicts a blood pump operating at 10,000 rpm, 3 L/min flow rate, and 52 mmHg pressure head. The high-speed blade rotation generates a pressure head that pushes the blood, resulting in lower inlet and higher outlet pressures. Fig. 8A shows the pressure distribution of the pump's inner wall, with region IV(the impeller) experiencing approximately 10^4Pa pressure due to blood rotation and blade work, while other regions exhibit a more uniform pressure distribution. Fig. 8B presents the pressure distribution on the guide head, impeller, and tail, revealing that the impeller blade's working face (regionV) and the guide blade's tail end (regionVI) experience around 10^4Pa pressure, which is reasonable.

Fig. 9 displays the wall shear stress distribution in model A at a rotational speed of 10000 rpm, flow rate of 3 L/min, and pressure head of 52 mmHg. As seen in Fig. 9A, high shear stress is concentrated at the guide head, impeller, and guide tail. The maximum shear stress occurs at the upstream positions of the impeller and guide tail blades. Chamfering at these positions during sample processing can alleviate shear stress concentration. The maximum shear stress also occurs locally at the guide head due to blood backflow between

Table 4
Reflux coefficient of different section.

Section	R (%)
I	0.12
II	0.16
III	0.03

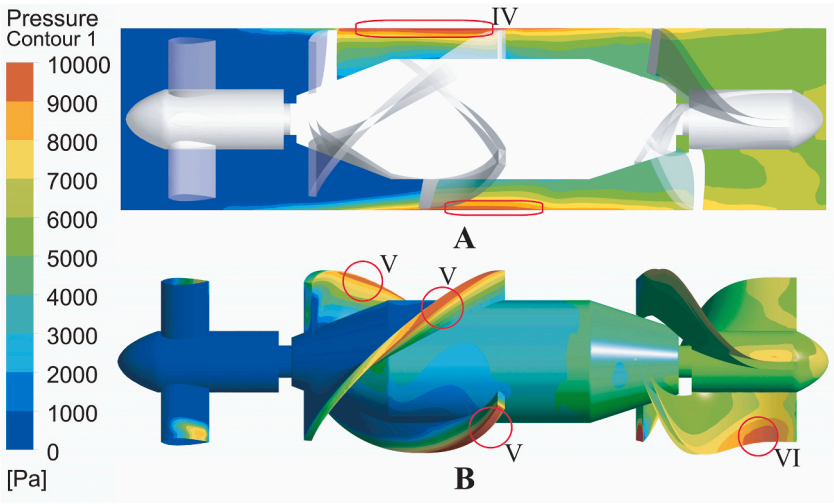

Fig. 8. (A) Pressure distribution map of the mid-section of the blood pump; (B) Pressure distribution map of the 3D model of the blood pump.

the guide head and impeller. Fig. 9B shows that approximately 95.08 % of the regions experience shear stress below 200 Pa, while only 1.56 % of the regions experience shear stress above 300 Pa. Therefore, areas with lower shear stress, which account for the majority of the distribution, induce less destructive blood flow in model A.

4. Discussion

Pediatric ventricular assist devices require careful blade design due to dimensional limitations. However, designing blades that meet multiple goals, such as hydraulic performance, hemodynamics, and hemolysis, based on various parameters poses a challenge. Traditional design methods, like the streamline method [38], are unsuitable for blood pump blade design. The streamline method focuses on the hydraulic performance and efficiency of axial flow pumps, originally developed for aircraft airfoils. In blood pump design, blade design must consider both the potential damage of high-speed rotating blades to blood and the overall hemodynamics of the pump.

In this study, we optimized the design of a blood pump blade using an orthogonal experiment method based on six parameters selected from CFD single factor variable experiments and design experience. Through 25 sets of orthogonal experiments and range analysis, we determined the order of influence of different parameters on the pump's pressure head and obtained a model pump with the optimal parameter combination. By reducing the blood pump speed from 12000 rpm to 10000 rpm, we mitigated the risk of hemolysis compared to the baseline pump.

CFD is a powerful technology for hydraulic design of blood pumps and numerical hemolysis assessment, avoiding the need for prototyping and blood experiments, reducing design time and cost. However, CFD-based hemolysis calculation accuracy is controversial, with limited ability to calculate the hemolysis value of the blood pump [39]. The key hemolysis model is empirical, such as the power law model [31] used in our study. Despite extensive research on hemolysis modeling [40–42], CFD-based calculations still differ significantly from experimental results. However, our study aims to compare hemolysis performance across different leaf parameter combinations, rather than predict the hemolysis value using CFD, making the use of an empirical hemolysis model justifiable.

In the velocity vector diagram of the blood pump, sections I, II and III exhibit partial reflux. The axial flow pump generates inevitable reflux when blood flow impinges on the blade, but the angle and range of reflux can be influenced by blade parameters. Optimization of these parameters can reduce flow loss, enhance hydraulic performance, and improve hemolysis performance of the blood pump. In Fig. 8, pressure is relatively high (10^4 Pa) on the inner wall of the blade region, impeller blade working face, and guide tail blade due to blade work and blood impact. This is a normal phenomenon, and there is no concentrated pressure distribution in local areas. Fig. 9 shows that the head of the impeller blade and guide tail blade exhibit concentrated shear stress distribution. Appropriate chamfering treatment in the corresponding position in the actual product can alleviate shear stress concentration and reduce the risk of hemolysis.

This study has some limitations. Firstly, the hemolysis evaluation lacks experimental verification and is purely numerical. We plan to conduct clinical haemolysis tests on the blood pump to address this. Secondly, future research can incorporate the haemolysis calculation value and key area reflux rate as design target values in an orthogonal experiment. This combined with haemolysis tests will lead to a more complete design method for pediatric blood pumps.

5. Conclusions

In this study, we investigated the impact of varying blade parameters on the pressure head of a pediatric blood pump using an

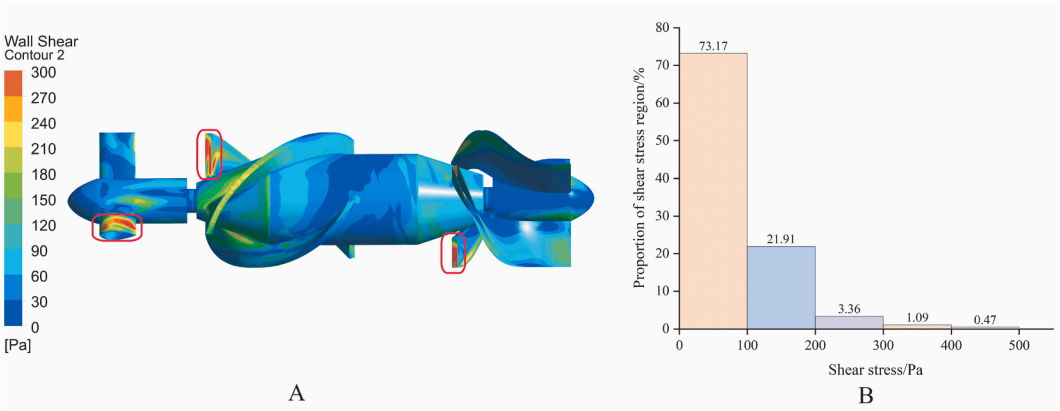

Fig. 9. (A) Shear stress distribution; (B) The proportion of different shear stress.

orthogonal experimental design. Through comparison of hydraulic performance and hemolysis across different models, we identified the optimal model and working conditions. Subsequently, we conducted hydraulic performance testing on the optimal model, which revealed a smooth H-Q curve and flow field, minimal reflux, uniform pressure distribution, and low shear stress and hemolysis levels as calculated by CFD analysis. Our findings offer valuable insights for the design of pediatric blood pumps.

CRediT authorship contribution statement

Kaiyun Gu: Writing – review & editing, Writing – original draft, Methodology, Data curation, Conceptualization. **Kaiyue Yang:** Writing – original draft, Validation, Software, Investigation, Data curation. **Changlong Zhao:** Validation, Investigation, Formal analysis. **Qiang Shu:** Writing – review & editing, Writing – original draft, Project administration, Conceptualization. **Ru Lin:** Writing – original draft, Project administration, Data curation, Conceptualization.

Data availability statement

The original contributions presented in the study are included in the article/supplementary material; further inquiries can be directed to the corresponding authors.

Ethics approval and consent to participate

Not applicable.

Consent for publication

Not applicable.

Funding

This work is supported by the National Natural Science Foundation of China (Grant No. 11902006).

Declaration of competing interest

The authors declare that they have no known competing financial interests or personal relationships that could have appeared to influence the work reported in this paper.

References

[1] R.E. Shaddy, A.T. George, T. Jaecklin, E.N. Lochlainn, L. Thakur, R. Agrawal, S. Solar-Yohay, F. Chen, J.W. Rossano, T. Severin, M. Burch, Systematic Literature review on the incidence and prevalence of heart failure in children and adolescents, Pediatr. Cardiol. 39 (2018) 415–436, https://doi.org/10.1007/s00246-017-1787-2.

[2] J. Sundström, S. Gustafsson, T. Cars, D. Lindholm, Heart failure treatment in the last years of life: a nationwide study of 364 000 individuals, Eur. J. Heart Fail. (2024), https://doi.org/10.1002/ejhf.3426, 10.1002/ejhf.3426. Advance online publication.

[3] J.W. Rossano, J.J. Kim, J.A. Decker, J.F. Price, F. Zafar, D.E. Graves, D.L. Morales, J.S. Heinle, B. Bozkurt, J.A. Towbin, S.W. Denfield, W.J. Dreyer, J.L. Jefferies, Prevalence, morbidity, and mortality of heart failure-related hospitalizations in children in the United States: a population-based study, J. Card. Fail. 18 (2012) 459–470, https://doi.org/10.1016/j.cardfail.2012.03.001.

[4] R.E. Andrews, M.J. Fenton, D.A. Ridout, M. Burch, British Congenital Cardiac Association,New-onset heart failure due to heart muscle disease in childhood: a prospective study in the United Kingdom and Ireland, Circulation 117 (2008) 79–84, https://doi.org/10.1161/CIRCULATIONAHA.106.671735.

[5] C.H. Tseng, The age- and sex-specific incidence and medical expenses of heart failure hospitalization in 2005 in Taiwan: a study using data from the National Health Insurance, J. Am. Geriatr. Soc. 58 (2010) 611–613, https://doi.org/10.1111/j.1532-5415.2010.02755.x.

[6] D. Kozik, B. Alsoufi, Pediatric mechanical circulatory support - a review, Indian J. Thorac. Cardiovasc. Surg. 39 (Suppl 1) (2023) 80–90, https://doi.org/10.1007/s12055-023-01499-3.

[7] A.I. Dipchand, R. Kirk, D.C. Naftel, E. Pruitt, E.D. Blume, R. Morrow, D. Rosenthal, S. Auerbach, M.E. Richmond, J.K. Kirklin, Pediatric heart transplant study investigators, ventricular assist device support as a bridge to transplantation in pediatric patients, J. Am. Coll. Cardiol. 72 (2018) 402–415, https://doi.org/10.1016/j.jacc.2018.04.072.

[8] D.L.S. Morales, I. Adachi, D.M. Peng, P. Sinha, A. Lorts, K. Fields, J. Conway, J.D. St Louis, R. Cantor, D. Koehl, J.P. Jacobs, J.K. Kirklin, E.D. Blume, J. W. Rossano, Pedimacs investigators, fourth annual pediatric interagency registry for mechanical circulatory support (Pedimacs) report, Ann. Thorac. Surg. 110 (2020) 1819–1831, https://doi.org/10.1016/j.athoracsur.2020.09.003.

[9] A. Di Molfetta, K. Zielinski, G. Ferrari, M. Kozarski, P. Okrzeja, R. Iacobelli, S. Filippelli, G. Perri, M. Darowski, M. Massetti, R. Jarvik, A. Amodeo, Is the new infant Jarvik 2015 suitable for Patients<8 kg? In vitro study using a hybrid simulator, Artif. Organs 43 (2019) E1–E8, https://doi.org/10.1111/aor.13302.

[10] R. Bryant, F. Zafar, C. Castleberry, J.L. Jefferies, A. Lorts, C. Chin, D.L. Morales, Transplant survival after Berlin heart EXCOR support, ASAIO J. 63 (2017) 80–85, https://doi.org/10.1097/MAT.0000000000000439.

[11] A. Di Molfetta, K. Zielinski, G. Ferrari, M. Kozarski, P. Okrzeja, R. Iacobelli, S. Filippelli, G. Perri, M. Darowski, M. Massetti, R. Jarvik, A. Amodeo, Is the new infant Jarvik 2015 suitable for Patients<8 kg? In vitro study using a hybrid simulator, Artif. Organs 43 (2019) E1–E8, https://doi.org/10.1111/aor.13302.

[12] R. Adorisio, M. Grandinetti, C. Giorni, D. Selvaggio, S. Filippelli, M. Trezzi, R. Iacobelli, G. Brancaccio, A. Amodeo, Preliminary data on the clinical use of infant Jarvik 2015 in children with dilated cardiomyopathy; recovery will be the new therapeutic goal? J. Heart Lung Transplant. 40 (2021) s175, https://doi.org/10.1016/j.healun.2021.01.515.

[13] Y. Li, J. Yu, H. Wang, Y. Xi, X. Deng, Z. Chen, Y. Fan, Investigation of the influence of blade configuration on the hemodynamic performance and blood damage of the centrifugal blood pump, Artif. Organs 46 (2022) 1817–1832, https://doi.org/10.1111/aor.14265.

[14] L. Wiegmann, S. Boës, D. de Zélicourt, B. Thamsen, M. Schmid Daners, M. Meboldt, V. Kurtcuoglu, Blood pump design variations and their influence on hydraulic performance and indicators of hemocompatibility, Ann. Biomed. Eng. 46 (2018) 417–428, https://doi.org/10.1007/s10439-017-1951-0.

[15] L.H. Tompkins, B.N. Gellman, G.F. Morello, S.R. Prina, T.J. Roussel, J.A. Kopechek, P.C. Petit, M.S. Slaughter, S.C. Koenig, K.A. Dasse, Design and computational evaluation of a pediatric MagLev rotary blood pump, ASAIO J. 67 (2021) 1026–1035, https://doi.org/10.1097/MAT.0000000000001323.

[16] S. Bozzi, S. Vesentini, M. Santus, N. Ghelli, P. Fontanili, M. Corbelli, G.B. Fiore, A.C.L. Redaelli, Fluid dynamics characterization and thrombogenicity assessment of a levitating centrifugal pump with different impeller designs, Med. Eng. Phys. 83 (2020) 26–33, https://doi.org/10.1016/j.medengphy.2020.07.008.

[17] B. Thamsen, U. Gülan, L. Wiegmann, C. Loosli, M. Schmid Daners, V. Kurtcuoglu, M. Holzner, M. Meboldt, Assessment of the flow field in the HeartMate 3 using three-dimensional particle tracking velocimetry and comparison to computational fluid dynamics, ASAIO J. 66 (2020) 173–182, https://doi.org/10.1097/MAT.0000000000000987.

[18] M. Chang, N. Hur, M. Moshfeghi, S. Kang, W. Kim, S.H. Kang, A numerical study on mechanical performance and hemolysis for different types of centrifugal blood pumps. The ASME 2015 International Mechanical Engineering Congress and Exposition, November 13-19, 2015, https://doi.org/10.1115/IMECE2015-53568. Houston.

[19] J.F. Antaki, M.R. Ricci, J.E. Verkaik, S.T. Snyder, T.M. Maul, J. Kim, D.B. Paden, M.V. Kameneva, B.E. Paden, P.D. Wearden, H.S. Borovetz, PediaFlow™ Maglev ventricular assist device: a Prescriptive design approach, Cardiovasc. Eng. 1 (1) (2010) 104–121, https://doi.org/10.1007/s13239-010-0011-9.

[20] V. Kannojiya, A.K. Das, P.K. Das, Proposal of hemodynamically improved design of an axial flow blood pump for LVAD, Med. Biol. Eng. Comput. 58 (2) (2020) 401–418, https://doi.org/10.1007/s11517-019-02097-5.

[21] B. Ghadimi, A. Nejat, S.A. Nourbakhsh, N. Naderi, Shape optimization of a centrifugal blood pump by coupling CFD with metamodel-assisted genetic algorithm, J. Artif. Organs 22 (1) (2019) 29–36, https://doi.org/10.1007/s10047-018-1072-z.

[22] C. Ozturk, I.B. Aka, I. Lazoglu, Effect of blade curvature on the hemolytic and hydraulic characteristics of a centrifugal blood pump, Int. J. Artif. Organs 41 (11) (2018) 730–737, https://doi.org/10.1177/0391398818785558.

[23] P. Wu, J. Huo, W. Dai, W.T. Wu, C. Yin, S. Li, On the optimization of a centrifugal Maglev blood pump through design variations, Front. Physiol. 12 (2021) 699891, https://doi.org/10.3389/fphys.2021.699891.

[24] Y.L. Zhang, K.Y. Zhang, Z.C. Zhu, Optimal design of impeller for self-priming pump based on orthogonal method, Sci. Rep. 13 (1) (2023) 16491, https://doi.org/10.1038/s41598-023-43663-0.

[25] H. Chang, W. Shi, W. Li, et al., Experimental optimization of jet self-priming centrifugal pump based on orthogonal design and grey-correlational method, J. Therm. Sci. 29 (2020) 241–250, https://doi.org/10.1007/s11630-019-1160-2.

[26] Z. Wang, C. Zhao, W. Zhang, Multi-objective design and optimization of squeezed branch pile based on orthogonal test, Sci. Rep. 13 (1) (2023) 22508, https://doi.org/10.1038/s41598-023-49936-y.

[27] Chen, Research on Hydraulic Suspension Structure Design and Blood Compatibility of Centrifugal Blood Pump [D], Harbin University of Science and Technology, 2023, https://doi.org/10.27063/d.cnki.ghlgu.2022.000730.

[28] J.D. Huo, Towards a High-Fidelity Simulation and Design Optimization of Rotary Blood Pumps Using Large Eddy Simulation, Suzhou University, 2022, https://doi.org/10.27351/d.cnki.gszhu.2022.002209 [D].

[29] Feng, Flow field simulation analysis and structural optimization design of rolling blood pump, J. Southeast Univ. (2022), https://doi.org/10.27014/,dcnki.Gdnau.2020.000893. The.

[30] C.S. Fox, T. Palazzolo, M. Hirschhorn, R.M. Stevens, J. Rossano, S.W. Day, V. Tchantchaleishvili, Throckmorton Al, Development of the centrifugal blood pump for a hybrid continuous flow pediatric total artificial heart: model, make, measure, Front. Cardiovas. Med. 9 (2022) 886874, https://doi.org/10.3389/fcvm.2022.886874.

[31] M.E. Taskin, K.H. Fraser, T. Zhang, C. Wu, B.P. Griffith, Z.J. Wu, Evaluation of Eulerian and Lagrangian models for hemolysis estimation, ASAIO J. 58 (2012) 363–372, https://doi.org/10.1097/MAT.0b013e318254833b.

[32] A. Garon, M.I. Farinas, Fast three-dimensional numerical hemolysis approximation, Artif. Organs 28 (2004) 1016–1025, https://doi.org/10.1111/j.1525-1594.2004.00026.x.

[33] A. Arvand, M. Hormes, H. Reul, A validated computational fluid dynamics model to estimate hemolysis in a rotary blood pump, Artif. Organs 29 (2005) 531–540, https://doi.org/10.1111/j.1525-1594.2005.29089.x.

[34] L. Ge, L.P. Dasi, F. Sotiropoulos, A.P. Yoganathan, Characterization of hemodynamic forces induced by mechanical heart valves: Reynolds vs. viscous stresses, Ann. Biomed. Eng. 36 (2008) 276–297, https://doi.org/10.1007/s10439-007-9411-x.

[35] H. Quan, Y. Guo, R. Li, Q. Su, Y. Chai, Optimization design and experimental study of vortex pump based on orthogonal test, Sci. Prog. 103 (1) (2020) 36850419881883, https://doi.org/10.1177/0036850419881883.

[36] W. Yu-Qin, D. Ze-Wen, Optimization design of hump phenomenon of low specific speed centrifugal pump based on CFD and orthogonal test, Sci. Rep. 12 (1) (2022) 12121, https://doi.org/10.1038/s41598-022-16430-w.

[37] Y.U.N. Xu, L.E.I. Tan, S. Cao, et al., Multiparameter and multiobjective optimization design of centrifugal pump based on orthogonal method[J]. Proceedings of the Institution of Mechanical Engineers, Part C, J. Mech. Eng. Sci. 231 (14) (2017) 2569–2579, https://doi.org/10.1177/0954406216640303.

[38] Z. Yu, J. Tan, S. Wang, B. Guo, Structural improvement study of streamline design method, conical hub, and auxiliary blades for axial blood pump, Int. J. Artif. Organs 44 (4) (2021) 251–261, https://doi.org/10.1177/0391398820959344.

[39] T. Zhang, M.E. Taskin, H.B. Fang, A. Pampori, R. Jarvik, B.P. Griffith, Z.J. Wu, Study of flow-induced hemolysis using novel Couette-type blood-shearing devices, Artif. Organs 35 (2011) 1180–1186, https://doi.org/10.1111/j.1525-1594.2011.01243.x.

[40] G. Heuser, R. Opitz, A Couette viscometer for short time shearing of blood, Biorheology 17 (1980) 17–24, https://doi.org/10.3233/bir-1980-171-205.
[41] L. Pauli, J. Nam, M. Pasquali, M. Behr, Transient stress-based and strain-based hemolysis estimation in a simplified blood pump, Int. J. Numer. Method. Biomed. Eng. 29 (2013) 1148–1160, https://doi.org/10.1002/cnm.2576.
[42] P. Hariharan, G. D'Souza, M. Horner, R.A. Malinauskas, M.R. Myers, Verification benchmarks to assess the implementation of computational fluid dynamics based hemolysis prediction models, J. Biomech. Eng. 137 (2015) 094501, https://doi.org/10.1115/1.4030823.